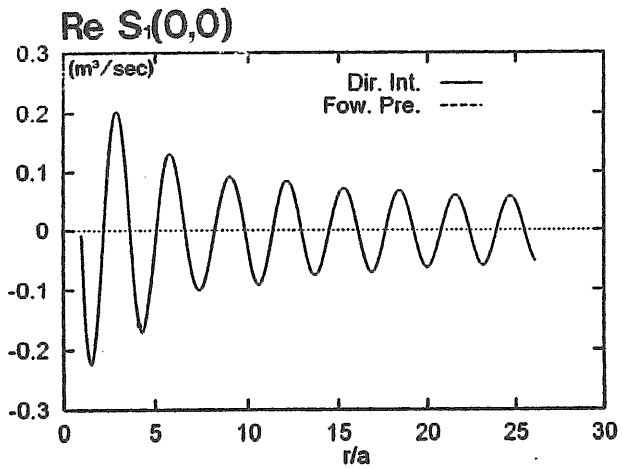

Fig. 3-A Real part of $S_1(0,0)$

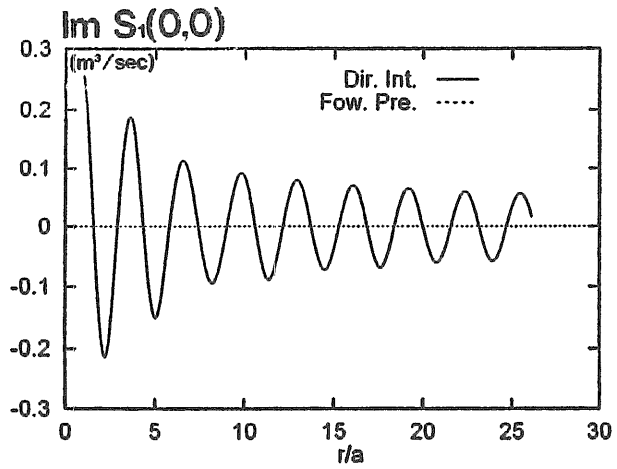

Fig. 3-B Imaginary part of $S_1(0,0)$

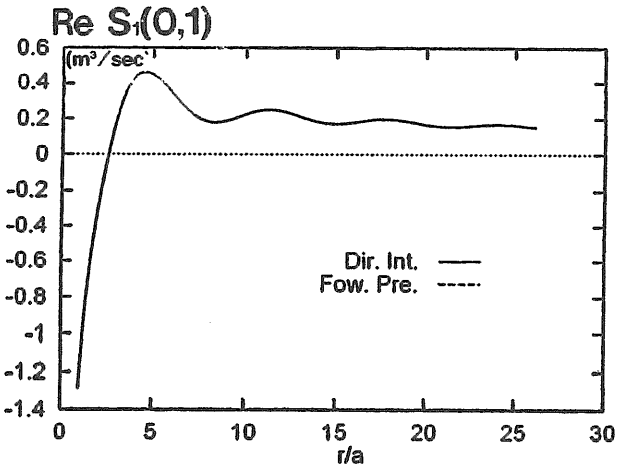

Fig. 3-C Real part of $S_1(0,1)$

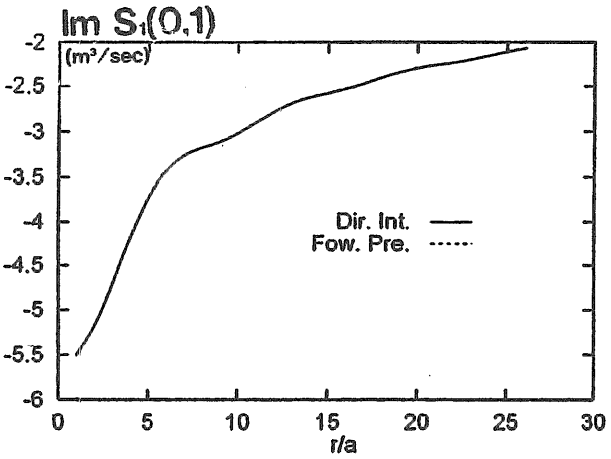

Fig. 3-D Imaginary part of $S_1(0,1)$

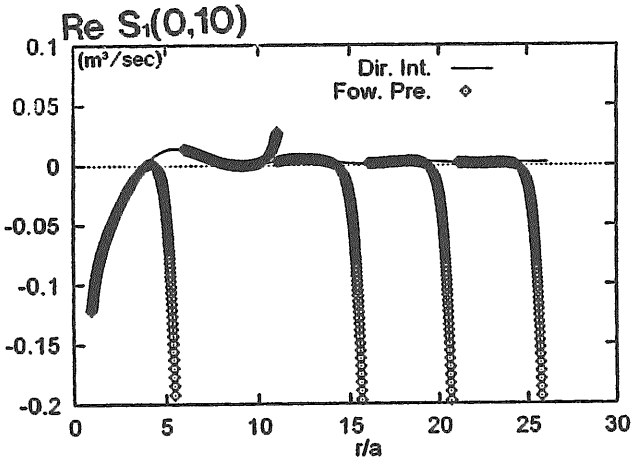

Fig. 3-E Real part of $S_1(0,10)$

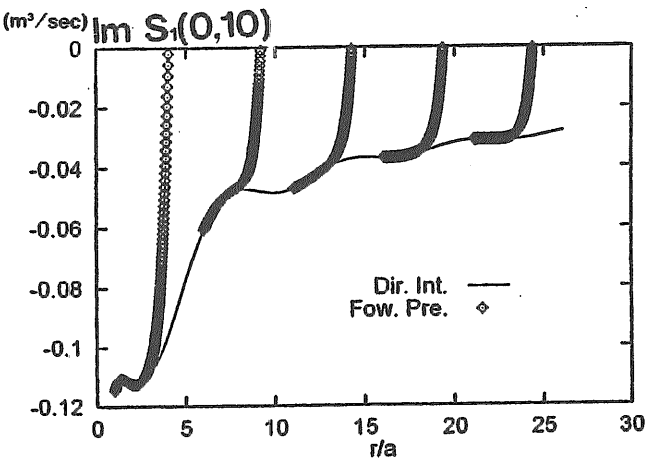

Fig. 3-F Imaginary part of $S_1(0,10)$

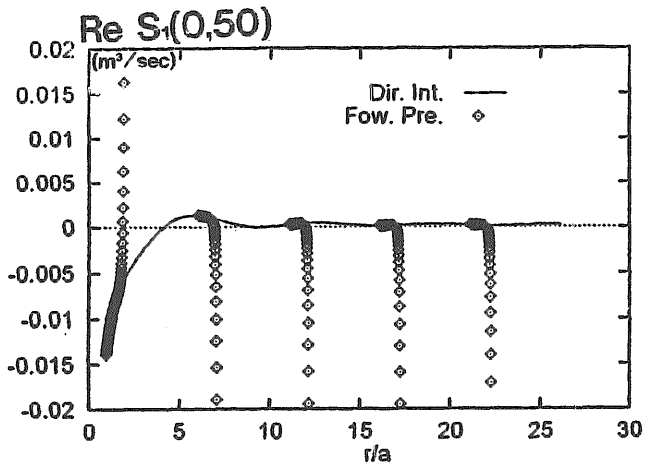

Fig. 3-G Real part of $S_1(0,50)$

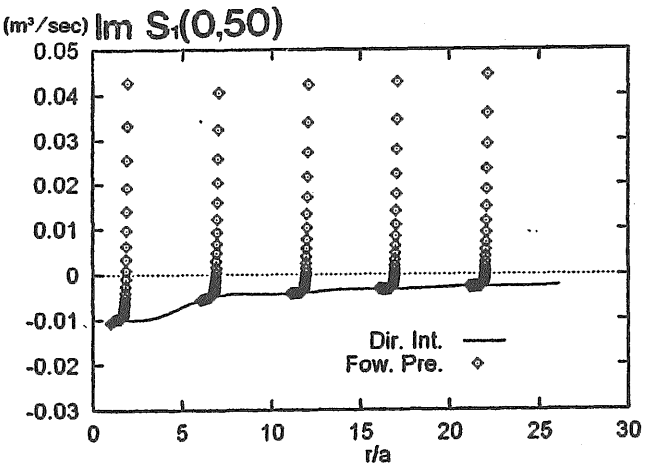

Fig. 3-H Imaginary part of $S_1(0,50)$

Figure 3. Examination on the methods, the direct integration method and forward predict method, for computing $S_1(m,n)$ for a uniform cylinder of radius a in a water depth of d/a=10; wave number ka=0.5.

For the *1*st, *10*th and *50*th eigen-modes of S_1 we apply the forward prediction method for every 400 steps, then correct it by the direct integration method. From the Figs. 3-C – 3-H, we can seen that for the first eigen-mode the forward prediction method can give accurate results in the 400 steps. For the *10*th eigen-mode the forward prediction method can give accurate results for some steps. After that the method will lose accuracy and diverges quickly. For the *50*th mode, the available distance to predict is shorter than the *10*th mode and the prediction method diverges more easily. The reason for long predictable length for low eigen-modes is that actually the dominating factor is the variable $\kappa_n \Delta r$ in modified Bessel functions rather than the distance Δr itself. Furthermore, the predictable length is also affected by a truncation-error tolerance

$$\int_{r_1}^{r_1+\Delta r} K_m(\kappa_n r) q_D^{(2)} r\,dr \Big/ \left[\int_{r_0}^{r_1} K_m(\kappa_n r) q_D^{(2)} r\,dr + \int_{r_1}^{r_1+\Delta r} K_m(\kappa_n r) q_D^{(2)} r\,dr\right] < Er \qquad (51)$$

used in calculation of the function S_1 by the direct integration method. In the present calculation, a tolerance of 1.0E-04 is applied.

Figure 4 shows the comparison between the direct integration and forward prediction method for the function S_2. The steps for the forward prediction method are exactly the same as for the function S_1. It can be seen that for the all of the four eigen-modes, the results from the two methods are exactly the same. The reason is that the forward prediction method for the function S_2 is successively accumulating, rather than subtracting as for S_1.

In practical calculation, the method used in computing S_1 is that firstly the direct integral method is used to compute the accurate values, then the forward prediction method is used to predict them for a certain steps. Then, the direct integration method is used again to remove the error accumulated in the forward prediction method and to guarantee that the forward prediction method can be used for the next loop. The numbers of steps used in the forward prediction method are different for each models, and are determined by a previous

numerical examination. This calculation loop is used repeatedly until the second order potential is obtained in the whole desired area.

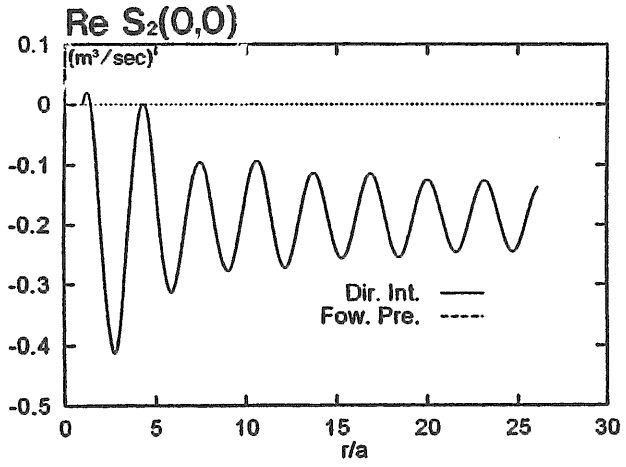

Fig. 4-A Real part of $S_2(0,0)$

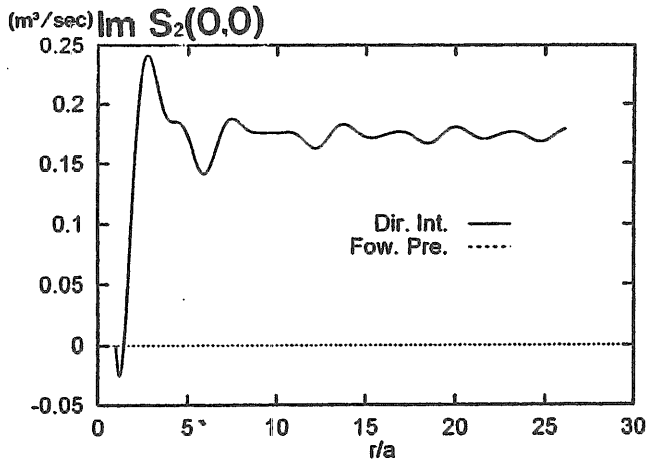

Fig. 4-B Imaginary part of $S_2(0,0)$

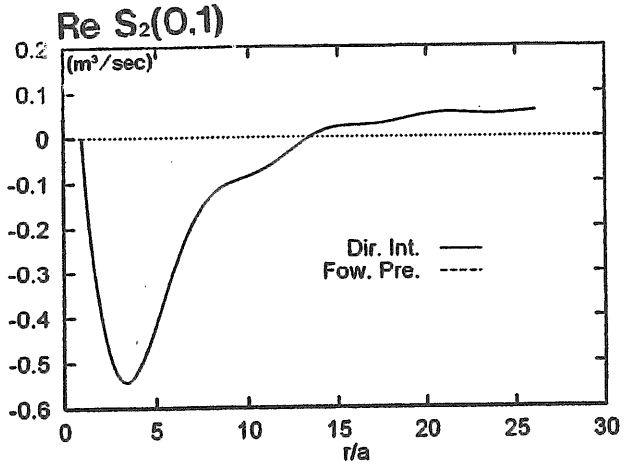

Fig. 4-C Real part of $S_2(0,1)$

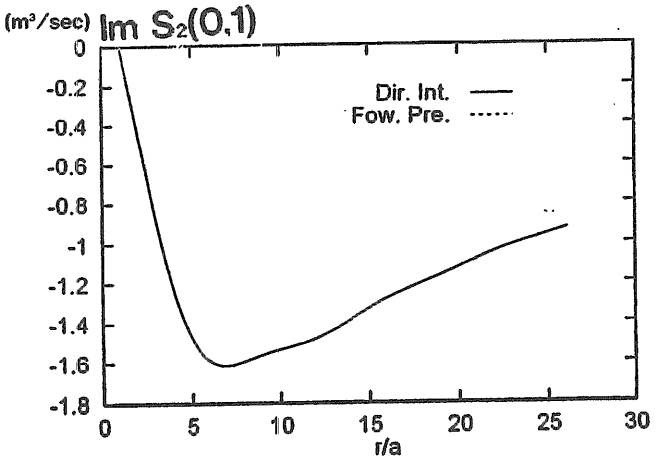

Fig. 4-D Imaginary part of $S_2(0,1)$

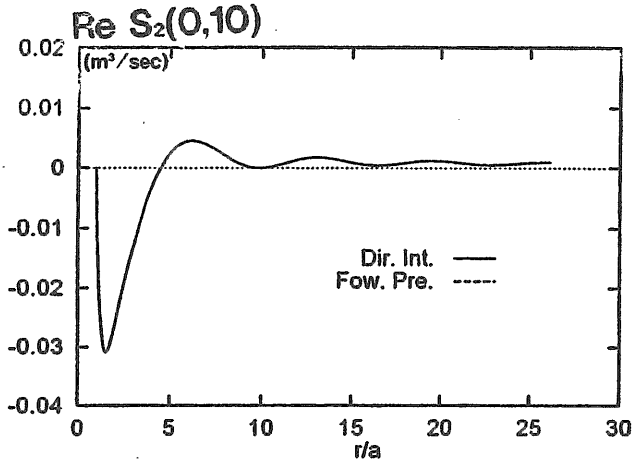

Fig. 4-E Real part of $S_2(0,10)$

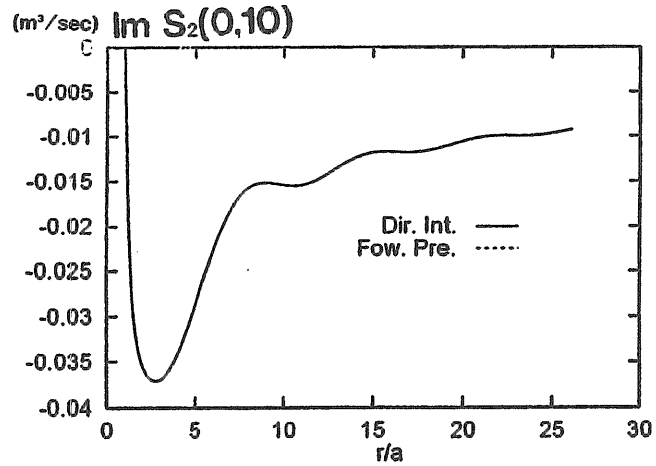

Fig. 4-F Imaginary part of $S_2(0,10)$

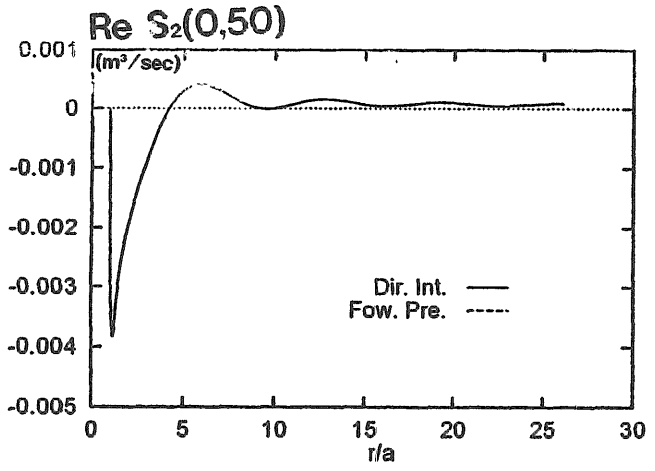

Fig. 4-G Real part of $S_2(0,50)$

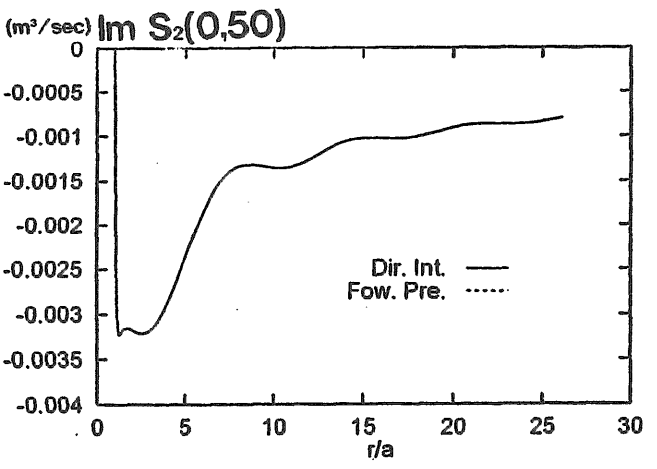

Fig. 4-H Imaginary part of $S_2(0,50)$

Figure 4. Examination on the methods, the direct integration method and forward predict method, for computing $S_2(m,n)$ for a uniform cylinder of radius a in a water depth of d/a=10; wave number ka=0.5.

6.3 Second order potential on the free surface

After having gotten those two functions S_1 and S_2, we can obtain the second order potential in fluid domain easily. Figure 5 shows the comparison of present results of second order diffraction potential on the free surface with Malenica's (1994) results. The comparison is made on the *0*th, *1*st and *5*th Fourier modes of diffraction potential, and also the radial derivative of the potential, which is obtained by a simple backward numerical differentiation.

It can be seen from the figures that the curves of potentials are very smooth, but the ones of radial derivatives have some noises. This is due to that some errors have been accumulated in the forward prediction method when the direct integration method is used to get an accurate value for the next computing loop. For the potential itself, this error is very small and can be tolerated. But, since the step is very small, the error of derivative will be quite big in the local area. To obtain a smooth result for the radial derivative, we have to use less steps to predict, or use other differentiation scheme.

From the comparison with Malenica's semi-analytic solution, it can be seen that for all the three modes of both potential and its derivative, the present results have a good agreement with Malenica's.

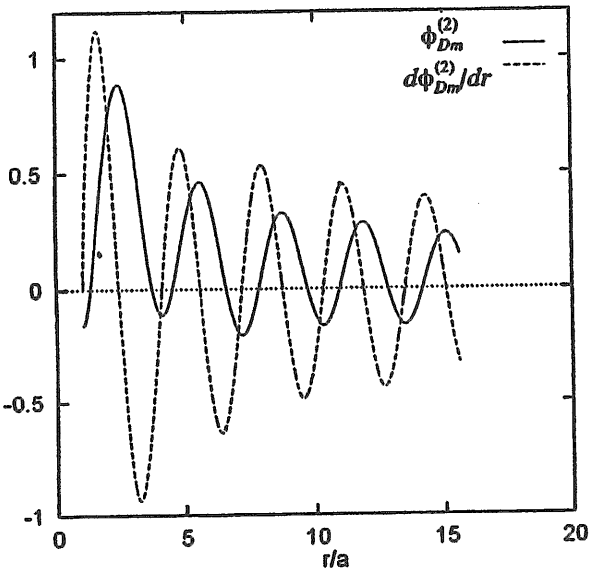

Fig. 5-A Real part of present results of $\phi_{Dm}^{(2)}$ and $d\phi_{Dm}^{(2)}/dr$, $m=0$

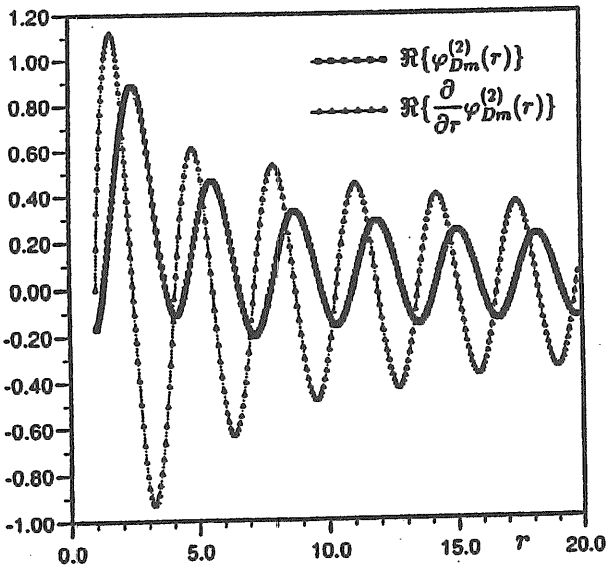

Fig. 5-B Real part of Malenica & Molin's results of $\phi_{Dm}^{(2)}$ and $d\phi_{Dm}^{(2)}/dr$, $m=0$

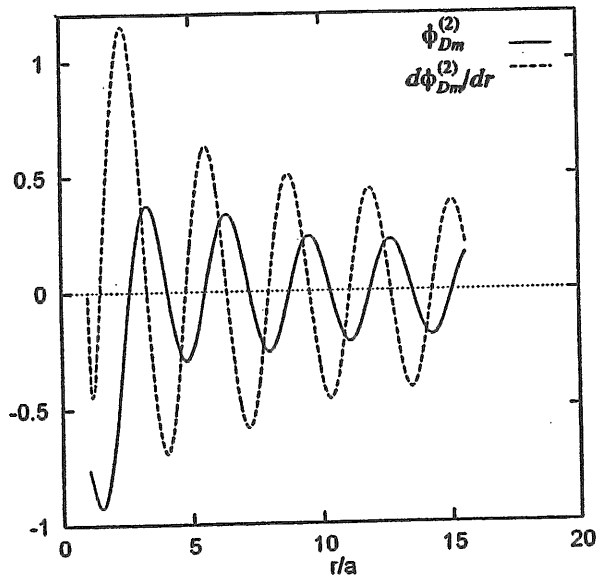

Fig. 5-C Imaginary part of present results of $\phi_{Dm}^{(2)}$ and $d\phi_{Dm}^{(2)}/dr$, $m=0$

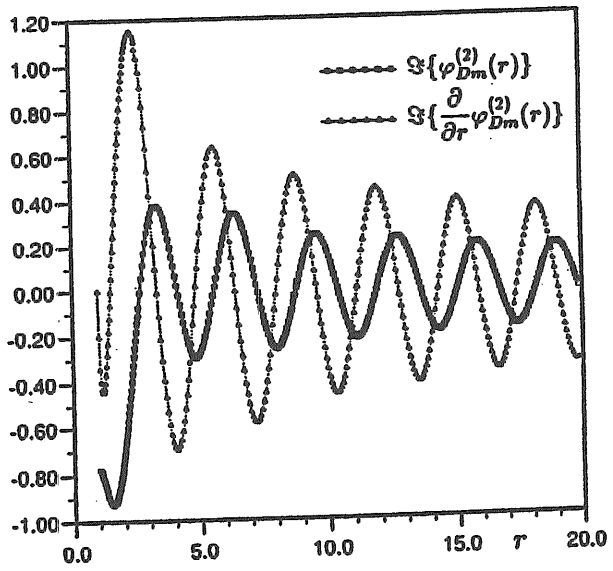

Fig. 5-D Imaginary part of Malenica & Molin's results of $\phi_{Dm}^{(2)}$ and $d\phi_{Dm}^{(2)}/dr$, $m=0$

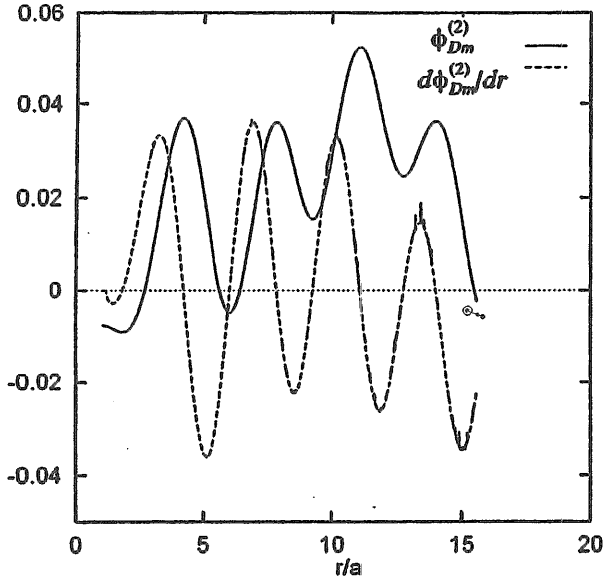

Fig. 5-E Real part of present results of $\phi_{Dm}^{(2)}$ and $d\phi_{Dm}^{(2)}/dr$, $m=1$

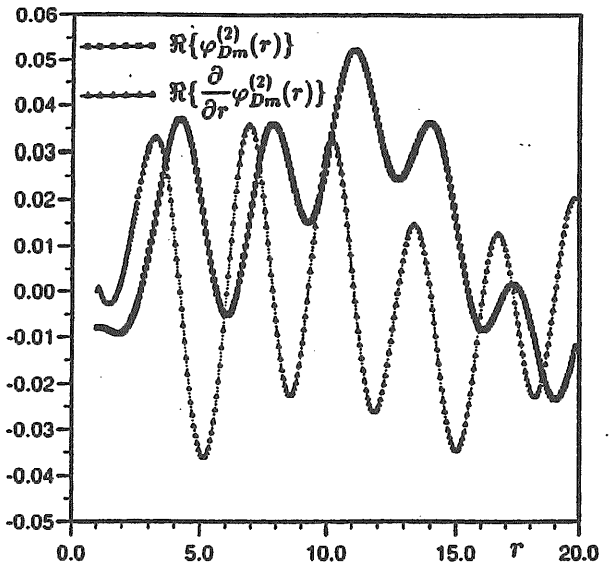

Fig. 5-F Real part of Malenica & Molin's results of $\phi_{Dm}^{(2)}$ and $d\phi_{Dm}^{(2)}/dr$, $m=1$

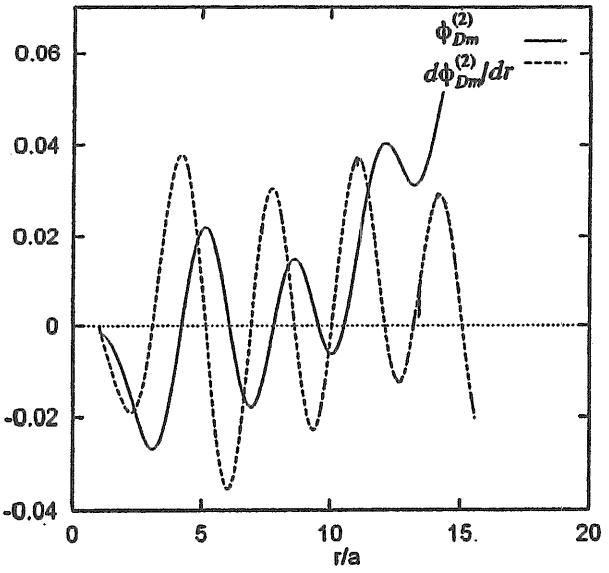

Fig. 5-G Imaginary part of present results of $\phi_{Dm}^{(2)}$ and $d\phi_{Dm}^{(2)}/dr$, $m=1$

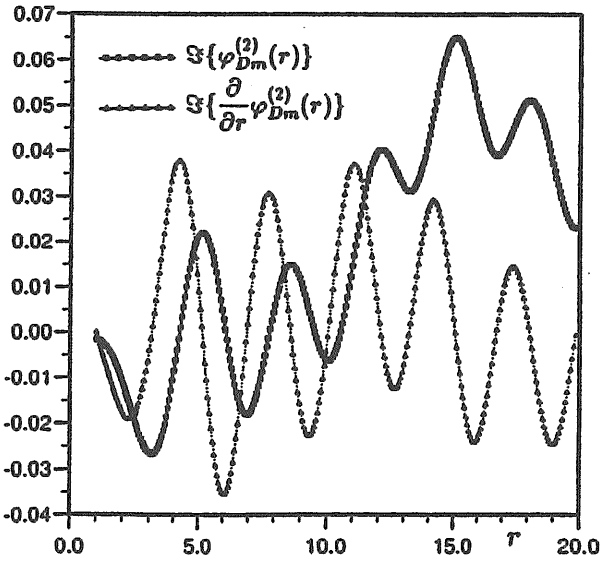

Fig. 5-H Imaginary part of Malenica & Molin's results of $\phi_{Dm}^{(2)}$ and $d\phi_{Dm}^{(2)}/dr$, $m=1$

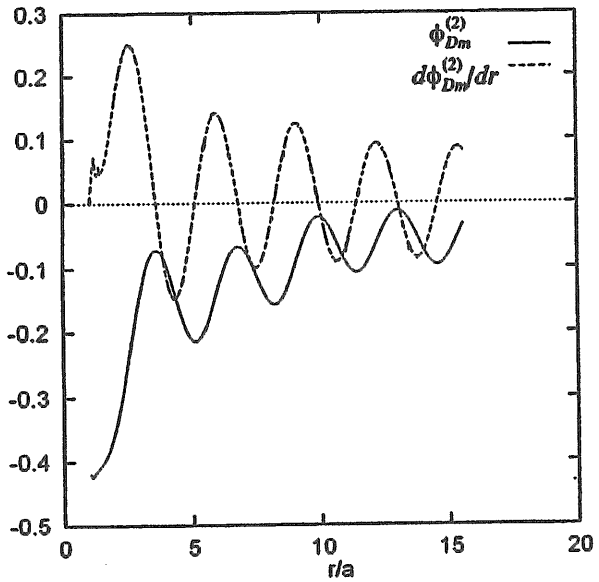

Fig. 5-I Real part of present results of $\phi_{Dm}^{(2)}$ and $d\phi_{Dm}^{(2)}/dr$, $m=5$

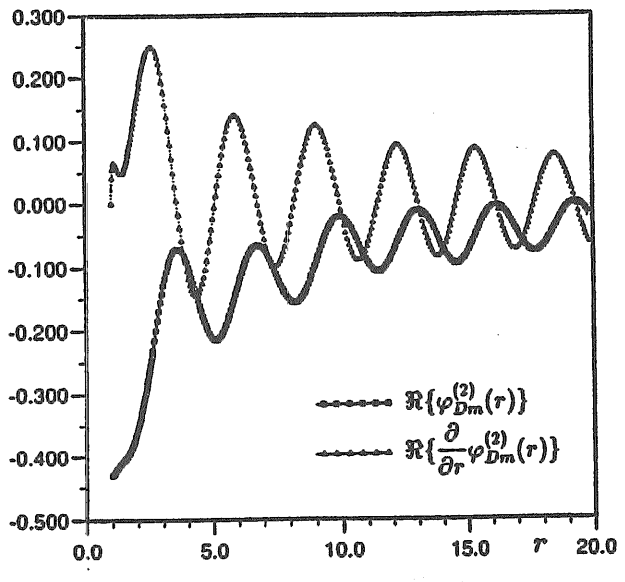

Fig. 5-J Real part of Malenica & Molin's results of $\phi_{Dm}^{(2)}$ and $d\phi_{Dm}^{(2)}/dr$, $m=5$

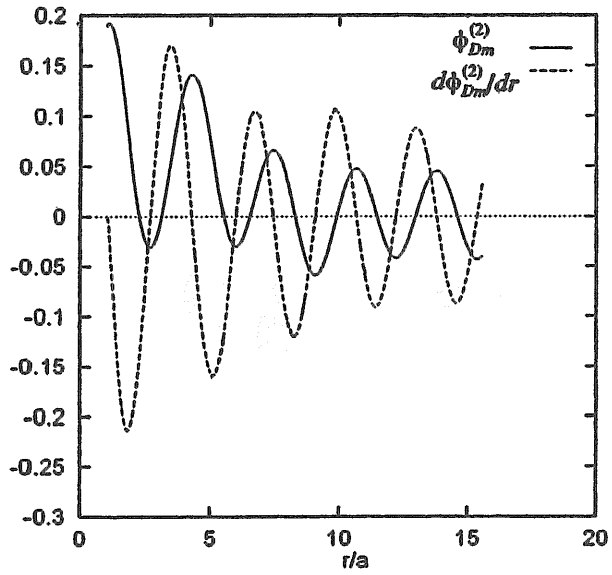

Fig. 5-K Imaginary part of present results of $\phi_{Dm}^{(2)}$ and $d\phi_{Dm}^{(2)}/dr$, $m=5$

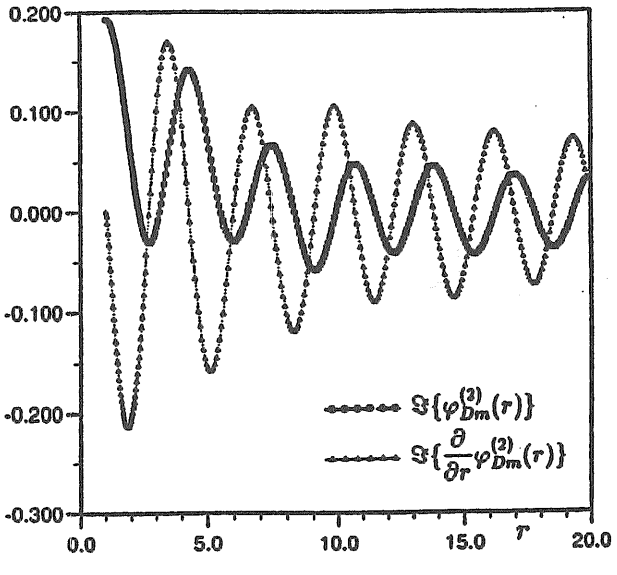

Fig. 5-L Imaginary part of Malenica & Molin's results of $\phi_{Dm}^{(2)}$ and $d\phi_{Dm}^{(2)}/dr$, $m=5$

Figure 5. Examination on second order diffraction potential and its radial derivative on the free surface for a uniform cylinder of radius a in a water depth of d/a=10; wave number ka=0.5.

6.4 Wave elevation

Figure 6 shows the second order wave elevation from the second order diffraction potential around a uniform cylinder. The water depth d/a=10; waves direct to positive x- direction with a wave number of ka=0.5. The pictures are plotted at every time step of one *16*th of wave period T_p ; that is one 8th of the second harmonic oscillation. Figure 7 shows the second order wave elevation from the diffraction potential around a truncated cylinder. The draft of the cylinder is T/a=1.0, and the water depth and the wave conditions are the same as for the uniform cylinder. From the comparison of figures 6 and 7, it can be seen that the diffraction wave from the uniform cylinder is much higher than the one from the truncated cylinder. It means that at present wave frequency the diffraction from the lower part of the cylinder is still quite strong, and uniform cylinders will not make a good substitution for truncated cylinders when considering ringing phenomenon in long waves.

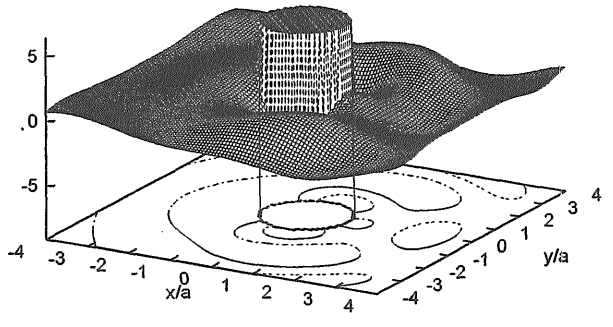

Fig. 6-A Wave elevation at t=0.0T_p

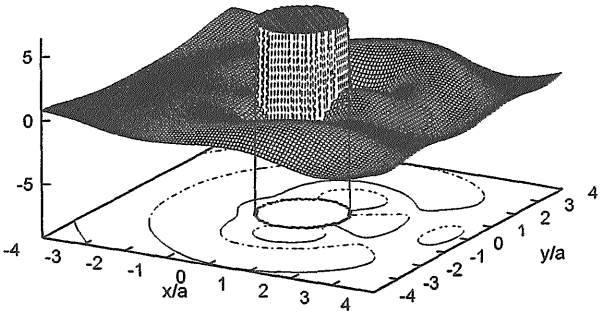

Fig. 6-B Wave elevation at t=T_p/16

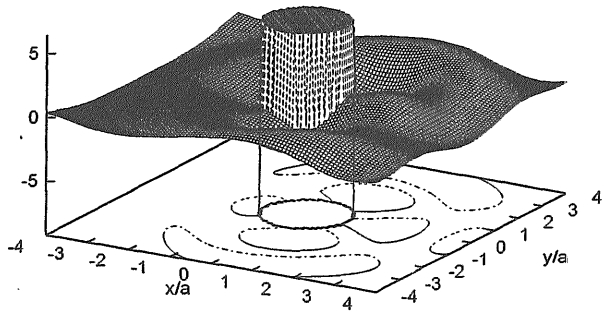

Fig. 6-C Wave elevation at t=2T_p/16

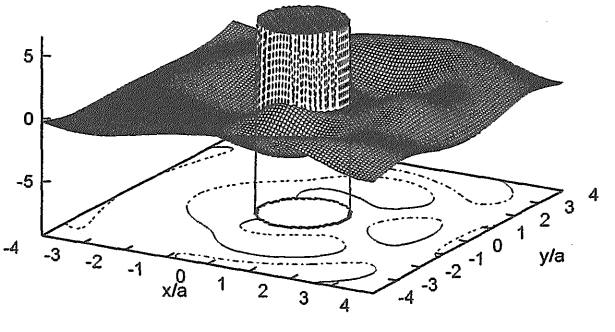

Fig. 6-D Wave elevation at t=3T_p/16

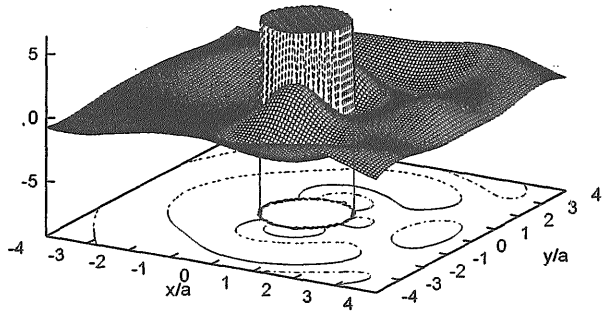

Fig. 6-E Wave elevation at t=4T_p/16

Figure 6. Wave elevation from second order diffraction potential around a uniform cylinder of radius a in a water depth of d/a=10; wave number ka=0.5.

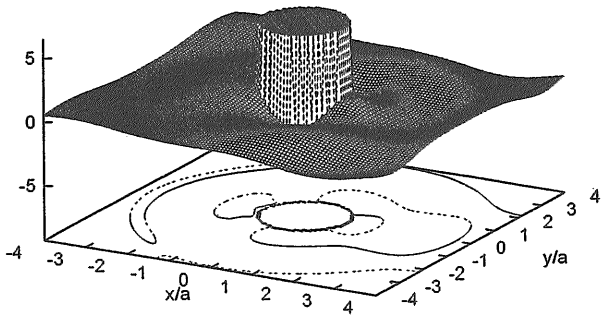

Fig. 7-A Wave elevation at t=0.0T_p

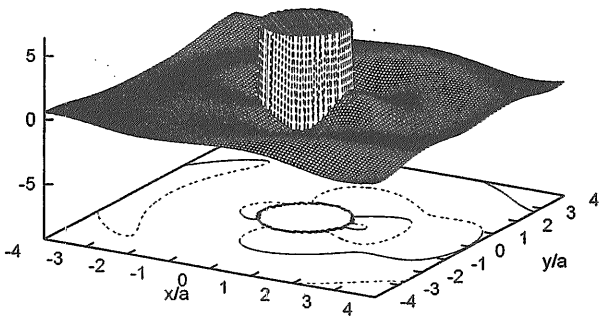

Fig. 7-B Wave elevation at t=T_p/16

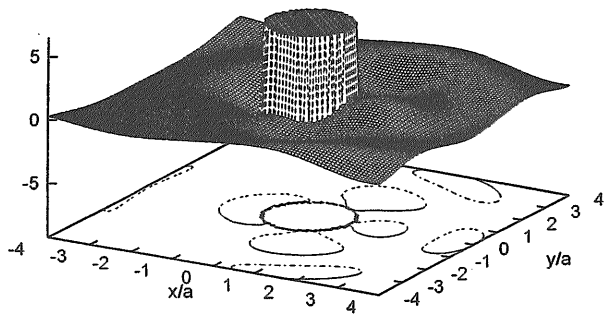

Fig. 7-C Wave elevation at t=2T_p/16

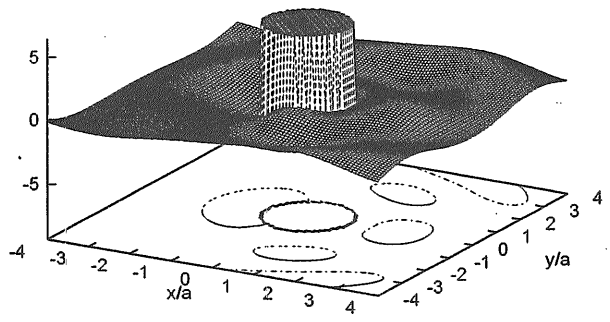

Fig. 7-D Wave elevation at t=3T_p/16

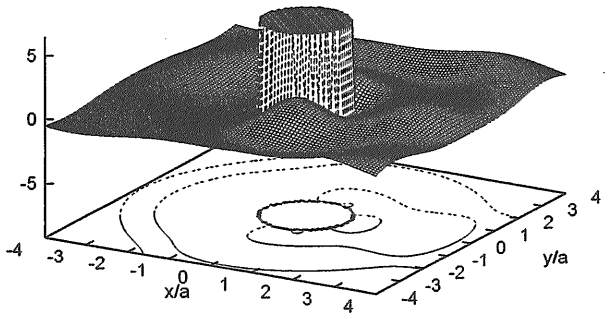

Fig. 7-E Wave elevation at t=4T_p/16

Figure 7. Wave elevation from second order diffraction potential around a truncated cylinder with radius a and draft T/a=1.0 in a water depth of d/a=10 ; wave number ka=0.5.

7. Conclusions

A complete second order diffraction solution has been derived for a vertical revolution body. The method is based on using the ring-source integral equation. The emphasis was laid on the quick calculation of the integration on the free surface. It can also be easily expanded for 3D arbitrary bodies. The following conclusions can be summarized.

1. The report derives an new integral equation for revolution bodies with vertical axes. The integral equation can cancel the leading term of the singularity in derivative of the ring- source. Remaining low order